

Programmable superpositions of Ising configurations

Lukas M. Sieberer¹ and Wolfgang Lechner^{2,3,*}

¹*Department of Physics, University of California, Berkeley, California 94720, USA*

²*Institute for Theoretical Physics, University of Innsbruck, A-6020 Innsbruck, Austria*

³*Institute for Quantum Optics and Quantum Information of the Austrian Academy of Sciences, A-6020 Innsbruck, Austria*
(Dated: June 6, 2018)

We present a framework to prepare superpositions of bit strings, i.e., many-body spin configurations, with deterministic programmable probabilities. The spin configurations are encoded in the degenerate ground states of the lattice-gauge representation of an all-to-all connected Ising spin glass. The ground state manifold is invariant under variations of the gauge degrees of freedom, which take the form of four-body parity constraints. Our framework makes use of these degrees of freedom by individually tuning them to dynamically prepare programmable superpositions. The dynamics combines an adiabatic protocol with controlled diabatic transitions. We derive an effective model that allows one to determine the control parameters efficiently even for large system sizes.

PACS numbers: 03.67.Ac,03.65.Ud,03.67.Bg

I. INTRODUCTION

The realization of quantum many-body superpositions is a cornerstone of current developments in quantum simulation experiments [1–8]. The aim is to achieve deterministic tunability over individual constituents of the quantum state in an experiment. Superpositions of bit strings (encoded in spin configurations) have been recently proposed as a key to quantum machine learning applications [9–11]. The challenge is thus to prepare a superposition of a polynomial number M bit strings in the 2^N -dimensional state space of N qubits. From an experimental point of view, the technique of adiabatic state preparation of spin models [12–15], which recently gained considerable interest as a tool to solve optimization problems, might serve as an effective method to prepare such states. If the ground state of the final Hamiltonian in an adiabatic protocol is energetically degenerate, the final state of the protocol is a superposition of the configurations in the degenerate manifold [16, 17]. However, the amplitudes of this state are governed by the details of the dynamics and the populations can be exponentially biased [18], leaving open the challenge to deterministically program these probabilities.

In this paper, we introduce a framework to generate superpositions of a polynomial number of bit strings with programmable squared amplitudes via an adiabatic-diabatic state preparation. The M different bit strings of length N are encoded in the ground-state manifold of the lattice-gauge representation of an all-to-all connected Ising model with $K = N(N - 1)/2$ spins [19]. Thus, a polynomial number M of configurations represent the ground-state manifold in an exponential 2^N -dimensional space.

We show that the gauge degrees of freedom in this representation, i.e., the constraints, allow one to shape

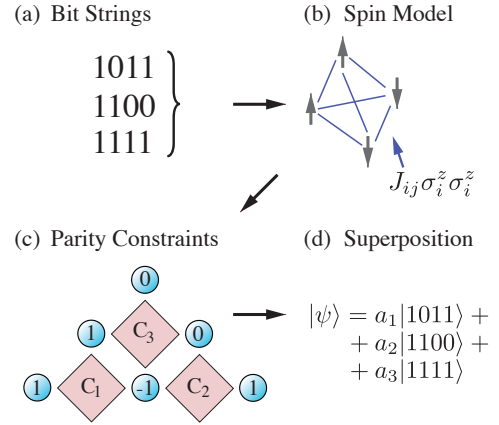


Figure 1. Schematic outline of the protocol to store classical bit strings in a quantum superposition with programmable probabilities $|a_n|^2$. (a) The input are M classical bit strings. (b) An all-to-all connected classical spin model with Hamiltonian $H = \sum_{i,j} J_{ij} \sigma_i^z \sigma_j^z$ is constructed such that the bit strings are its degenerate ground states. (c) The spin model is translated to a lattice gauge model with qubits (blue spheres) and with four-body constraint strengths C_p (red squares) [19]. (d) The adiabatic passage of this model yields a superposition of the M degenerate ground states. The probabilities can be tuned on demand by choosing the values of the C_p appropriately.

the quantum dynamics and program the final amplitudes of these M configurations. We develop an effective M -dimensional theory. In the reduced Hilbert space of the effective model, the parameters can be determined efficiently, even for system sizes that cannot be solved on current classical computers (i.e., more than 50 qubits).

The remainder of this paper is organized as follows: We begin in Sec. II by describing our state preparation protocol. Section III is devoted to a detailed account of the key step of the protocol, i.e., the adiabatic-diabatic dynamics leading to the desired superposition state, and

* w.lechner@uibk.ac.at

its description in terms of an effective model. An example that illustrates the method is presented in Sec. IV. We conclude in Sec. V and provide an outlook on future research directions.

II. PROTOCOL

The basis of the protocol is the lattice-gauge representation of an all-to-all connected spin model [19–23],

$$H(t) = -A(t) \sum_{i=1}^K \sigma_i^x - B(t) \sum_{i=1}^K J_i \sigma_i^z - C(t) \sum_{p=1}^{K-N+1} C_p \sigma_{n_p}^z \sigma_{w_p}^z \sigma_{s_p}^z \sigma_{e_p}^z. \quad (1)$$

Here, $\sigma_i^{x,y,z}$ are the Pauli operators acting on spins which are arranged on a two-dimensional square lattice with sites i , $K = N(N-1)/2$, and the sum in the last term runs over the $K-N+1$ constraints. Each constraint with index p involves the spins in the north, west, south, and east of the constraint site, as is indicated in Eq. (1) with subscripts n_p, w_p, s_p , and e_p . The functions $A(t) = t/T$ and $B(t) = C(t) = 1-t/T$ are linear switching functions, and T is the run time of the protocol. Initially, $A(0) = 1$ and $B(0) = C(0) = 0$, while at the end of the protocol $A(T) = 0$ and $B(T) = C(T) = 1$. We measure energies (and inverse times) in units of the transverse field strength, which is thus set to one. The qubits in Eq. (1) represent connections between logical spins of the all-to-all connected Ising model. In the mapping to the lattice-gauge representation, additional degrees of freedom are introduced, which are then removed by the constraints in the last term of Eq. (1) (see Ref. [19] for details). The constraint strengths C_p are gauge degrees of freedom. Tuning each of them individually does not change the low-energy subspace in the final Hamiltonian in which the bit strings are encoded. Thus the model features $(N-2)(N-3)/2$ additional parameters as compared to the original spin-glass formulation. We use these additional parameters to systematically design the quantum paths of an adiabatic-diabatic protocol, which allows us to program the squared amplitudes of the configurations in the final state.

Our protocol, which is illustrated in Fig. 1, aims at storing a polynomial number M of bit strings $x_n = 01011\dots$ where $n = 1, \dots, M$, as a quantum superposition state $|\psi\rangle = a_1|x_1\rangle + a_2|x_2\rangle + \dots$ with programmable probabilities $p_n = |a_n|^2$. This superposition state thus encodes classical data corresponding both to the bit strings x_n and the corresponding probabilities p_n . We regard the states $|x_n\rangle = |01011\dots\rangle$ as product states in the σ^z basis, with individual bits $x_{n,i} = 0, 1$ corresponding to eigenvalues ± 1 of σ_i^z .

The protocol consists of the following steps:

- (i) The bit strings are encoded as degenerate ground

states of a classical spin model [see Fig. 1 (a) and (b)]. This is achieved with a Hamiltonian of the form $H = \sum_{n=1}^M |x_n\rangle\langle x_n|$ which can be approximated, for example, via plated solutions [24] or Hopfield networks [25] in the form of an all-to-all connected model with energy $\sum_{i,j} J_{ij} \sigma_i^z \sigma_j^z$. The details of different strategies of this classical encoding will be discussed elsewhere [26]. We note that in this step a polynomial number of configurations is selected out of a 2^N -dimensional space.

- (ii) This spin Hamiltonian is reformulated in the parity-constraint model introduced in Ref. [19] with Hamiltonian $H(t)$ in Eq. (1) [see Fig. 1 (c)]. Logical bit strings x_n are thus translated to physical bit strings z_n , representing spin configurations in the lattice-gauge model.
- (iii) The key step, and focus of this work, is the dynamics that leads to the desired superposition. The system is initialized in the trivial and non-degenerate ground state of $H(0)$, in which all spins are aligned by the transverse field. Evolution with $H(t)$ yields a superposition of all configurations in the ground state manifold of $H(T)$, $|\psi\rangle = \sum_{n=1}^M a_n |z_n\rangle$, where the probabilities $|a_n|^2$ can be tuned on demand by adjusting the control parameters C_p . These parameters C_p are determined from static properties of an effective Hamiltonian, and can be fine-tuned via an iterative protocol. Note that only a polynomial number of parameters is required as M is assumed to be polynomial.

III. EFFECTIVE MODEL

The quantum dynamics during step (iii) of the protocol can be understood in terms of a simple effective model which we derive in the following. In Secs. III A and III B, we introduce the adiabatic manifold and the effective Hamiltonian, based on the observation that during a slow sweep in the time-dependent Hamiltonian (1) the evolution is restricted to a manifold of the lowest-lying instantaneous energy eigenstates. The effective Hamiltonian governing the dynamics within this manifold can be determined by a Schrieffer-Wolff transformation, which we describe in Sec. III C. Using the effective Hamiltonian we determine the control parameters for the protocol in Secs. III D and III E.

A. Adiabatic-diabatic dynamics

The quantum adiabatic algorithm with a single non-degenerate ground state of the “problem Hamiltonian” $H(T)$ is successful if adiabaticity is maintained throughout the time evolution. Here, in contrast, we consider the case of an M -fold degenerate ground state manifold of the

problem Hamiltonian [18]. Thus, the gap closes as $t \rightarrow T$ and the dynamics can never be fully adiabatic. Nevertheless, by making T large, transitions out of the *adiabatic manifold* (AMF), which is spanned by the M lowest-lying instantaneous eigenstates $\{|\varphi_n(t)\rangle \mid n = 1, \dots, M\}$ of $H(t)$ and evolves for $t \rightarrow T$ into the degenerate ground state manifold of $H(T)$, are suppressed. Our protocol aims at controlling the *adiabatic dynamics within the AMF* by tuning the constraint strengths C_p . In this sense, the final state is prepared *adiabatic-diabatically*.

Within the AMF, the dynamics consists of two different regimes: up to a characteristic time t_d the dynamics is adiabatic and the system remains in the instantaneous ground state $|\varphi_1(t)\rangle$; from t_d to T the dynamics can be considered as a sudden quench of the Hamiltonian parameters, during which the state of the system $|\psi(t)\rangle$ essentially remains frozen, i.e., $|\psi(T)\rangle \approx |\psi(t_d)\rangle \approx |\varphi_1(t_d)\rangle$. (In the last equality, we omitted dynamical and Berry phases since we are interested solely in programming the *probabilities* of the final superposition state.) A detailed discussion of this Kibble-Zurek-inspired [27] approximation in the context of the Landau-Zener problem is provided in Ref. [28]. The *dynamical* problem of controlling diabatic transitions is thus (at least approximately) reduced to the *static* problem of choosing the constraint strengths C_p to tune the composition of the instantaneous ground state $|\varphi_1(t_d)\rangle$ at time t_d . Below, we derive the effective Hamiltonian $H_{\text{eff}}(t)$ in the AMF that allows us to do this efficiently. The characteristic time scale t_d can also be determined within the effective model as described in Sec. III D.

B. Derivation of the effective model

To put what we have described so far on a more formal base, we decompose the total Hilbert space as $\mathcal{H} = \mathcal{P}(t) \oplus \mathcal{Q}(t)$, where $\mathcal{P}(t)$ is the AMF that is spanned by the M lowest-lying instantaneous eigenstates, $|\varphi_n(t)\rangle$ with $n = 1, \dots, M$, of the lattice-gauge Hamiltonian $H(t)$ (1). These states become degenerate for $t \rightarrow T$, and consequently the dynamics within $\mathcal{P}(t)$ becomes diabatic, whereas a finite gap between the energies of the states in $\mathcal{P}(t)$ and higher-lying excited states spanning the subspace $\mathcal{Q}(t)$ is maintained throughout the protocol. Hence, transitions out of the AMF $\mathcal{P}(t)$ can be suppressed effectively by choosing the run time T of the protocol large enough. Strictly speaking, states within $\mathcal{P}(t)$ are also degenerate with states of $\mathcal{Q}(t)$ at $t = 0$. However, the system is initialized in the instantaneous ground state which is non-degenerate at $t = 0$ and separated from all excited states by a finite gap, so there are no diabatic transitions at short times. A state $|\psi(t)\rangle \in \mathcal{P}(t)$ can be written as

$$|\psi(t)\rangle = \sum_{n=1}^M \alpha_n(t) |\varphi_n(t)\rangle, \quad (2)$$

and the Schrödinger equation, projected to $\mathcal{P}(t)$, takes the form

$$i\dot{\alpha}_n(t) = \sum_{n'=1}^M A_{nn'}(t)\alpha_{n'}(t), \quad (3)$$

$$A_{nn'}(t) = \langle \varphi_n(t) | \left(H(t) - i \frac{d}{dt} \right) | \varphi_{n'}(t) \rangle.$$

The dynamics within the AMF is thus governed by the matrix elements $A_{nn'}(t)$ which are in turn determined by the instantaneous eigenstates $|\varphi_n(t)\rangle$. Finding these states by diagonalizing $H(t)$ can be achieved in a two-step procedure: (i) The space $\mathcal{P}(t)$ of the M lowest-lying states is decoupled from excited state space $\mathcal{Q}(t)$ by a Schrieffer-Wolff (SW) transformation $U_{\text{SW}}(t)$ [29]. As we describe in detail in Sec. III C, the SW transformation can be obtained as a perturbative expansion in the transverse field. (ii) The resulting effective Hamiltonian $H_{\text{eff}}(t) = U_{\text{SW}}(t)H(t)U_{\text{SW}}^\dagger(t)$ is diagonalized within the reduced space by applying another unitary transformation $U_0(t)$. Hence, the instantaneous eigenstates of $H(t)$ that span $\mathcal{P}(t)$ can be written as

$$|\varphi_n(t)\rangle = U_{\text{SW}}^\dagger(t)U_0^\dagger(t)|z_n\rangle. \quad (4)$$

Inserting this representation in Eq. (3) we obtain

$$A_{nn'}(t) = \langle z_n | \left[U_0(t) \left(H_{\text{eff}}(t) - iU_{\text{SW}}(t)\dot{U}_{\text{SW}}(t)^\dagger \right) \times U_0(t)^\dagger - iU_0(t)\dot{U}_0(t)^\dagger \right] |z_{n'}\rangle. \quad (5)$$

While the perturbative expansion of $U_{\text{SW}}(t)$ can be derived without specifying the exact superposition state that should be prepared [which is encoded in the local field term in Eq. (1)], the unitary transformation $U_0(t)$ explicitly depends on these details. For this reason it is more convenient to work in a basis in which H_{eff} is not diagonal, i.e.,

$$\beta_n(t) = \sum_{n'=1}^M \langle z_n | U_0^\dagger(t) |z_{n'}\rangle \alpha_{n'}(t). \quad (6)$$

Then, the Schrödinger equation (3) takes the form

$$i\dot{\beta}_n(t) = \sum_{n'} B_{nn'}(t)\beta_{n'}(t), \quad (7)$$

where

$$B_{nn'}(t) = \langle z_n | \left(H_{\text{eff}}(t) - iU_{\text{SW}}(t)\dot{U}_{\text{SW}}^\dagger(t) \right) |z_{n'}\rangle. \quad (8)$$

Due to the derivative with respect to time, the second term in this matrix element is suppressed by an additional factor of $1/T$ (recall that T is the dimensionless run time of the protocol measured in units of the inverse local field strength), and can thus be dropped [30]. Then, in its simplest form, the effective model is given by the equation of motion in Eq. (6) with

$$B_{nn'}(t) \approx \langle z_n | H_{\text{eff}}(t) |z_{n'}\rangle. \quad (9)$$

We note, however, that including the second term in $B_{nn'}(t)$ to make the effective model more accurate is straightforward. Having specified the dynamics within the AMF and its description in terms of an effective Hamiltonian, we proceed to discuss the perturbative expansion of the SW transformation $U_{\text{SW}}(t)$.

C. Calculation of the effective Hamiltonian

The SW transformation $U_{\text{SW}}(t)$ decouples the AMF $\mathcal{P}(t)$ from the manifold of excited states $\mathcal{Q}(t)$. To find $U_{\text{SW}}(t)$, we can treat the transverse field in the time-dependent Hamiltonian (1) as a perturbation. Clearly, such an expansion could not be justified at early times of the evolution when $A(t) \approx 1$ while $B(t), C(t) \ll 1$ and the transverse field is the dominant part of the Hamiltonian (1). However, as explained in Sec. III A, we require our effective model to be accurate only at t_d when the dynamics becomes diabatic. This is the case towards the end of the protocol when the strength of the transverse field $A(t_d)$ becomes small and the gaps between the states $|\varphi_n(t)\rangle$ spanning the AMF close. Moreover, below we will see that each order in perturbation theory is accompanied by an additional factor of $1/C_p$ for one of the constraints $p = 1, \dots, K - N + 1$ in Eq. (1), i.e., the effective expansion parameter is $A(t_d)/C_p$ — which is small by construction of the lattice-gauge formulation [19]. We emphasize, however, that we use perturbation theory only to construct $U_{\text{SW}}(t)$ and thus solve the *static* problem of finding the instantaneous eigenstates of $H(t)$, whereas the *dynamics* is fundamentally non-perturbative (in the sense that it cannot be described by, e.g., adiabatic perturbation theory [31]).

Let us now consider the structure of the ensuing perturbative expansion. The unperturbed Hamiltonian $H_0(t)$ comprises the local fields and the four-body constraints in Eq. (1),

$$H_0(t) = \frac{t}{T} (H_J + H_C), \quad (10)$$

where

$$H_J = - \sum_{i=1}^K J_i \sigma_i^z, \quad H_C = - \sum_{p=1}^{K-N+1} C_p \sigma_{n_p}^z \sigma_{w_p}^z \sigma_{s_p}^z \sigma_{e_p}^z, \quad (11)$$

while the perturbation is given by the transverse field,

$$V(t) = \left(1 - \frac{t}{T}\right) \sum_{i=1}^K \sigma_i^x, \quad (12)$$

and the total Hamiltonian is thus

$$H(t) = H_0(t) + V(t). \quad (13)$$

$H_0(t)$ is diagonal in a basis of σ^z -product states. In particular, the states $|z_n\rangle$ where $n = 1, \dots, M$ span the degenerate ground state manifold \mathcal{P}_0 of $H_0(t)$. The ground

state manifold \mathcal{P}_0 coincides with the AMF at the end of the protocol when $t = T$, i.e., $\mathcal{P}(T) = \mathcal{P}_0$ and thus $U_{\text{SW}}(T) = \mathbb{1}$, while at any $t < T$, the SW transformation is a direct rotation between $\mathcal{P}(t)$ and \mathcal{P}_0 [32]. Then, the effective Hamiltonian defined by $H_{\text{eff}}(t) = U_{\text{SW}}(t)H(t)U_{\text{SW}}^\dagger(t)$ is block-diagonal when written in the basis of eigenstates of $H_0(t)$ — which, as pointed out above, is just the basis of σ^z -product states. In other words, the SW transformation $U_{\text{SW}}(t)$ decouples the space $\mathcal{P}(t)$ from the space of excited states $\mathcal{Q}(t)$ by incorporating the effect of virtual transitions to $\mathcal{Q}(t)$ in the effective Hamiltonian $H_{\text{eff}}(t)$.

The form of the perturbative expansion of $H_{\text{eff}}(t)$ is particularly transparent since the perturbation $V(t)$, which is the sum of terms σ_i^x , has the effect of flipping single physical spins. In other words, applying the perturbation once to a state $|z_n\rangle$ yields a superposition of states at a Hamming distance of one, where the Hamming distance is measured with respect to the encoded bit string z_n . The transverse field $V(t)$ thus (i) modifies the energies (i.e., the diagonal elements of the effective Hamiltonian) of the states $|z_n\rangle$ at second order in perturbation theory and (ii) couples states $|z_n\rangle$ and $|z_{n'}\rangle$ (i.e., it generates off-diagonal elements of H_{eff}) at the order of their Hamming distance $h_{nn'}$. The second effect (ii) can be understood by noting that applying the perturbation V once to the state $|z_n\rangle$ flips a single spin and therefore it has to be applied $h_{nn'}$ times to connect the states $|z_n\rangle$ and $|z_{n'}\rangle$. We further note, that since the qubits of the lattice-gauge representation encode the relative orientation of spins in the original all-to-all spin glass model [19], flipping a single spin of a state in \mathcal{P} always yields a state in $\mathcal{Q}_0 = \mathcal{Q}(T)$ (thus leading to an additional factor of $1/C_p$ in the perturbative expansion as asserted above). For this reason, Hamming distances between ground states are at least two, and hence the lowest non-trivial order in perturbation theory that contributes to $H_{\text{eff}}(t)$ is two. From this discussion, we can already infer that the matrix elements $H_{\text{eff},nn'}(t) = \langle n|H_{\text{eff}}(t)|n'\rangle$ of the effective Hamiltonian take the following form to leading order in perturbation theory:

$$\begin{aligned} H_{\text{eff},nn}(t) &= \frac{t}{T} e_0 + \frac{T}{t} \left(1 - \frac{t}{T}\right)^2 e_n, \\ H_{\text{eff},nn'}(t) &= \left(\frac{T}{t}\right)^{h_{nn'}-1} \left(1 - \frac{t}{T}\right)^{h_{nn'}} g_{nn'}, \end{aligned} \quad (14)$$

Here, te_0/T is the ground-state energy of $H_0(t)$, which according to Eq. (10) depends linearly on time. The time dependence of the other terms reflects the general structure of perturbation theory: For each order of the perturbative expansion is a factor of $1 - t/T$, i.e., the strength of the transverse field at time t , while the factors T/t stem from the energy denominators, which are differences of eigenenergies of the unperturbed Hamiltonian $H_0(t)$. We note that the divergence of the factors T/t for $t \rightarrow 0$ need not bother us since as discussed above we are interested primarily in the effective Hamiltonian

at $t = t_d$. Below we describe how the coefficients e_n and $g_{nn'}$ can be obtained explicitly. They are given in Eqs. (27), (28), and (29) for a specific example. For Hamming distances $h_{nn'} > 2$, we note that the off-diagonal elements in Eq. (14) vanish faster $\sim (1 - t/T)^{h_{nn'}}$ than the diagonal ones $\sim (1 - t/T)^2$ as $t \rightarrow T$. Therefore, the instantaneous eigenstates $|\varphi_n(t)\rangle$ converge to the states $|z_n\rangle$ — and, in particular, not to linear combinations of these states. This corroborates that preparing a superposition of the states $|z_n\rangle$ dynamically relies crucially on diabatic transitions.

After these preliminaries, let us explicitly specify the perturbative expansion, i.e., the calculation of e_n and $g_{nn'}$ in Eq. (14). We adopt the notation of Ref. [32], and all results for the SW we use in the following can be found there. In what follows, we denote by $P = \sum_{n=1}^M |z_n\rangle \langle z_n|$ the projector on the ground-state manifold \mathcal{P}_0 , and by $Q = \mathbb{1} - P$ the projector on the excited state space \mathcal{Q}_0 . These projectors commute with the unperturbed Hamiltonian, $[P, H_0] = [Q, H_0] = 0$. The ground state energy is E_0 , i.e., we have $H_0 |z_n\rangle = E_0 |z_n\rangle$. According to Eq. (10), E_0 depends linearly on time. However, for simplicity, we suppress the dependence on time of both H_0 and E_0 . Since the aim of the SW transformation is to decouple $\mathcal{P}(t)$ and $\mathcal{Q}(t)$, i.e., to bring the Hamiltonian to block-diagonal form, it is useful to introduce the following superoperators:

$$\mathcal{D}(X) = PXP + QXQ, \quad \mathcal{O}(X) = PXQ + QXP. \quad (15)$$

An operator X is block-diagonal (block-off-diagonal) iff $\mathcal{D}(X) = X$ ($\mathcal{O}(X) = X$). Any operator can be decomposed into block-diagonal and block-off-diagonal components. In particular, for the perturbation we have

$$V = V_d + V_{od}, \quad V_d = \mathcal{D}(V), \quad V_{od} = \mathcal{O}(V). \quad (16)$$

Finally, for the present case in which all states in \mathcal{P}_0 are degenerate, the superoperator \mathcal{L} defined in Ref. [32] takes the simple form

$$\mathcal{L}(X) = PX \frac{Q}{E_0 - H_0} - \frac{Q}{E_0 - H_0} XP. \quad (17)$$

Explicit expressions for $H_{\text{eff}}(t)$ up to fourth order in perturbation theory are given in Ref. [32], and we repeat them here for completeness. This order of perturbation theory is sufficient for the example discussed below which involves ground states with Hamming distances three and four. Higher orders — that are required to treat systems with ground states with larger Hamming distances — can be obtained through a systematic iterative procedure. The general form of the effective Hamiltonian to fourth order in perturbation theory is as follows:

$$\begin{aligned} H_{\text{eff}}^{(0)} &= H_0 P, & H_{\text{eff}}^{(2)} &= \frac{1}{2} P [S_1, V_{od}] P, \\ H_{\text{eff}}^{(1)} &= PVP, & H_{\text{eff}}^{(3)} &= \frac{1}{2} P [V_{od}, \mathcal{L}([V_d, S_1])] P, \end{aligned} \quad (18)$$

and

$$\begin{aligned} H_{\text{eff}}^{(4)} &= \frac{1}{2} P \left(\frac{1}{4} [S_1, [S_1, [S_1, V_{od}]] \right. \\ &\quad \left. - [V_{od}, \mathcal{L}([V_d, \mathcal{L}([V_d, S_1])])] \right) P, \end{aligned} \quad (19)$$

where $S_1 = \mathcal{L}(V_{od})$ is the first-order term in the perturbative expansion of the generator $S = \ln(U_{\text{SW}})$ of the Schrieffer-Wolff transformation [32]. For Hamming distances three and four between the degenerate ground states in the example considered below, there are some further simplifications. To name an example, we have $PVP = 0$, while $PVQVP$ has only diagonal elements, and $PVQVQVP$ is purely off-diagonal with non-vanishing elements between states with Hamming distance three etc. Using these simplifications we find:

$$\begin{aligned} H_{\text{eff}}^{(0)} &= E_0 P, & H_{\text{eff}}^{(2)} &= PV \frac{Q}{E_0 - H_0} VP, \\ H_{\text{eff}}^{(1)} &= 0, & H_{\text{eff}}^{(3)} &= P \left(V \frac{Q}{E_0 - H_0} \right)^2 VP, \end{aligned} \quad (20)$$

and

$$\begin{aligned} H_{\text{eff}}^{(4)} &= P \left(V \frac{Q}{E_0 - H_0} \right)^3 VP \\ &\quad - \frac{1}{2} \left[PV \left(\frac{Q}{E_0 - H_0} \right)^2 VPV \frac{Q}{E_0 - H_0} VP \right. \\ &\quad \left. + PV \frac{Q}{E_0 - H_0} VPV \left(\frac{Q}{E_0 - H_0} \right)^2 VP \right]. \end{aligned} \quad (21)$$

We note that $H_{\text{eff}}^{(0)}$, $H_{\text{eff}}^{(2)}$, and the last two terms in $H_{\text{eff}}^{(4)}$ are diagonal whereas $H_{\text{eff}}^{(3)}$ and the first term in $H_{\text{eff}}^{(4)}$ have non-zero elements only away from the diagonal. In the following, we omit the subleading diagonal contributions to H_{eff} stemming from $H_{\text{eff}}^{(4)}$. Then, the matrix elements of the effective Hamiltonian,

$$\begin{aligned} H_{\text{eff},nn} &= E_0 + \langle z_n | V \frac{Q}{E_0 - H_0} V | z_n \rangle, \\ H_{\text{eff},nn'} &= \langle z_n | \left(V \frac{Q}{E_0 - H_0} \right)^{h_{nn'}-1} V | z_{n'} \rangle, \end{aligned} \quad (22)$$

take the simple form reported in Eq. (14) above. In particular, the coefficients e_n and $g_{nn'}$ can be written as

$$e_n = \frac{t}{T} \left(1 - \frac{t}{T} \right)^{-2} \langle z_n | V \frac{Q}{E_0 - H_0} V | z_n \rangle, \quad (23)$$

and

$$\begin{aligned} g_{nn'} &= \left(\frac{t}{T} \right)^{h_{nn'}-1} \left(1 - \frac{t}{T} \right)^{-h_{nn'}} \\ &\quad \times \langle z_n | \left(V \frac{Q}{E_0 - H_0} \right)^{h_{nn'}-1} V | z_{n'} \rangle. \end{aligned} \quad (24)$$

We note that from the expressions for $H_0(t)$ in Eq. (10) and $V(t)$ in Eq. (12) it is evident that e_n and $g_{nn'}$ do not depend on time. However, the constraint strengths C_p enter both E_0 and H_0 and thus allow us to tune the matrix elements of the effective Hamiltonian. Consequently, also the composition of the eigenstates of $H_{\text{eff}}(t)$ can be adjusted and, following the logic outlined in Sec. III A, we use this freedom to ensure that the instantaneous ground state at the time t_d , at which the dynamics becomes diabatic, equals the superposition state we seek to prepare.

Before we proceed to estimate the time scale t_d , we note that the effective model, applied to the original all-to-all spin glass formulation, also provides a general framework to address the problem of fair sampling of degenerate ground states through quantum annealing [16, 18]. In particular, for spin-glass benchmark instances with controlled ground-state degeneracy, the effective model can be used to obtain the output state of quantum annealing with little computational effort. It is straightforward to extend the effective model to study the impact of, e.g., more complex driving Hamiltonians, on the composition of the output state. As we have shown here, in the lattice-gauge formulation, fair sampling can be achieved due to the additional ‘‘tuning knobs’’ provided by the parameters C_p .

D. Estimation of t_d

To estimate the time t_d at which the dynamics within the AMF becomes diabatic, we treat the approach for $t \rightarrow T$ of each pair of levels $E_n(t) - E_{n'}(t) \rightarrow 0$ where $n, n' = 1, \dots, M$ as an individual Landau-Zener problem. The latter is characterized by a time-dependent velocity and gap [33]:

$$v_{nn'} = \left| \frac{d}{dt} (H_{\text{eff},nn} - H_{\text{eff},n'n'}) \right|, \quad \Delta_{nn'} = H_{\text{eff},nn'}, \quad (25)$$

and t_d is determined by the usual criterion that separates the diabatic from the adiabatic regime in the Landau-Zener problem, $v_{nn'}/\Delta_{nn'}^2 = \pi$. Of all t_d found in this way for different pairs of levels n and n' , the smallest value indicates which transition becomes diabatic first. In general, transitions with higher Hamming distances have larger t_d . For the determination of the control parameters, i.e., the constraint strengths, we use the smallest value.

E. Determination of control parameters

Now we have all the tools at hand to determine the parameters C_p that lead to a final state $|\psi(T)\rangle = \sum_{n=1}^M a_n |z_n\rangle$ with the required probabilities $p_n = |a_n|^2$. One has to calculate the ground state $|\varphi_1(t_d)\rangle = \sum_{n=1}^M b_n |z_n\rangle$ of $H_{\text{eff}}(t_d)$ and find the values C_p that min-

imize the cost function

$$\Omega(\{b_n\}) = \sum_{n=1}^M \left(|b_n|^2 - p_n \right)^2. \quad (26)$$

This gives the desired result since $|\psi(T)\rangle \approx |\varphi_1(t_d)\rangle$ and thus $a_n \approx b_n$ as explained above. For a given choice of the probabilities p_n , typically the minimum of the cost function obtained in this way is $\Omega(\{b_n\}) \approx 0$, which means that within our approximate treatment the desired superposition could be prepared with fidelity close to one. We investigate whether this is true for any set of probabilities systematically for a specific example in Sec. IV C below. To further improve the fidelity of the solution, one can iteratively optimize the values of the C_p . In each iteration, the time evolution with $H_{\text{eff}}(t)$ is calculated to obtain the final state $|\psi(T)\rangle$ beyond the sudden quench approximation, and the C_p are updated to minimize the cost function $\Omega(\{a_n\})$ evaluated for the final state [34]. As noted below Eq. (14), the perturbative expansion of $H_{\text{eff}}(t)$ diverges for $t \rightarrow 0$. This, however, turns out to not be a severe obstacle in practice: for the iterative optimization of the constraint strengths C_p , we initialize the time evolution at a finite time $t_0 > 0$ in the instantaneous ground state $|\varphi_1(t_0)\rangle$. In the examples we considered, we found that the optimized C_p are almost insensitive to the value of t_0 for $0 < t_0 \lesssim t_d$. Since the optimization is carried out in the effective M -dimensional model, it can be done efficiently even if the dimension of the total physical Hilbert space 2^K is so large that the state preparation cannot be simulated on a classical computer but still be performed on a quantum device.

IV. EXAMPLE

Having described the protocol and the determination of the control parameters in detail, let us now illustrate the method by the example shown in Fig. 1. We take $M = 3$ bit strings $x_1 = 1011$, $x_2 = 1100$, and $x_3 = 1111$, and for demonstration we prepare superpositions of the states $|x_n\rangle$ with target probabilities $p_n = 1/M$ as well as $p_1 = 0.2$, $p_2 = 0.3$, and $p_3 = 0.5$.

A. Preparation of superposition states

In step (i) of the protocol described in Sec. II, these bit strings are encoded as the ground states of the Hamiltonian $H = \sum_{i,j} J_{ij} \sigma_i^z \sigma_j^z$ with $J_{12} = J_{13} = J_{34} = 1$, $J_{23} = -1$ and $J_{14} = J_{24} = 0$. The full energy landscape of H is shown in Fig. 2 (a), where the global \mathbb{Z}_2 symmetry is broken by an additional local field of strength $h = 1$. In step (ii) we switch to the lattice-gauge representation [19] featuring $K = 6$ qubits and three constraints as depicted in Fig. 1 (c). Due to the specific arrangement of the qubits, the constraints with strengths C_1 and C_2

are three-body interactions and C_3 is a four-body interaction (see Appendix A for details). Figure 2 (b) shows the time-dependent spectrum of the Hamiltonian (1) with $C_1 = C_2 = C_3 = 4$. To determine the values we have to assign to these parameters in order to prepare spe-

cific superposition states in step (iii) of the protocol, we have to determine the effective Hamiltonian $H_{\text{eff}}(t)$. For this example, the matrix elements of $H_{\text{eff}}(t)$ are given by Eq. (14) with the following coefficients on the diagonal (details of the calculation are given in Appendix A):

$$\begin{aligned} e_1 &= \frac{1}{2} \left(-\frac{1}{1+C_2} - \frac{1}{C_3} - \frac{1}{1+C_1+C_3} - \frac{1}{C_2+C_3} + \frac{1}{1-C_1-C_2-C_3} - \frac{1}{1+C_1} \right), \\ e_2 &= \frac{1}{2} \left(-\frac{1}{1+C_2} - \frac{1}{C_3} + \frac{1}{1-C_1-C_3} - \frac{1}{C_2+C_3} - \frac{1}{1+C_1+C_2+C_3} - \frac{1}{1+C_1} \right), \\ e_3 &= \frac{1}{2} \left(-\frac{1}{1+C_2} - \frac{1}{C_3} - \frac{1}{1+C_1+C_3} - \frac{1}{C_2+C_3} - \frac{1}{1+C_1+C_2+C_3} + \frac{1}{1-C_1} \right), \end{aligned} \quad (27)$$

and on the off-diagonal:

$$\begin{aligned} g_{13} &= \frac{1}{2^2} \left(-\frac{\frac{1}{C_2+C_3} + \frac{1}{1+C_1}}{1+C_1+C_2+C_3} - \frac{\frac{1}{1-C_1-C_2-C_3} - \frac{1}{C_2+C_3}}{1-C_1} + \frac{\frac{1}{1-C_1-C_2-C_3} - \frac{1}{1+C_1}}{C_2+C_3} \right), \\ g_{23} &= \frac{1}{2^2} \left(-\frac{\frac{1}{1+C_1} + \frac{1}{C_3}}{1+C_1+C_3} + \frac{\frac{1}{1-C_1-C_3} - \frac{1}{1+C_1}}{C_3} - \frac{\frac{1}{1-C_1-C_3} - \frac{1}{C_3}}{1-C_1} \right), \end{aligned} \quad (28)$$

and

$$\begin{aligned} g_{12} &= \frac{1}{2^3} \left(\frac{-\frac{\frac{1}{C_2+C_3} + \frac{1}{1+C_1+C_3}}{1+C_1+C_2} + \frac{\frac{1}{1-C_1-C_2-C_3} - \frac{1}{1+C_1+C_3}}{C_2} - \frac{\frac{1}{1-C_1-C_2-C_3} - \frac{1}{C_2+C_3}}{1-C_1}}{C_3} \right. \\ &\quad - \frac{-\frac{\frac{1}{C_2+C_3} - \frac{1}{C_3}}{C_2} - \frac{\frac{1}{1-C_1-C_2-C_3} - \frac{1}{C_2+C_3}}{1-C_1} - \frac{\frac{1}{1-C_1-C_2-C_3} - \frac{1}{C_3}}{1-C_1-C_2}}{1-C_1-C_3} \\ &\quad + \frac{-\frac{\frac{1}{1+C_1+C_3} + \frac{1}{C_3}}{1+C_1} + \frac{\frac{1}{1-C_1-C_2-C_3} - \frac{1}{1+C_1+C_3}}{C_2} - \frac{\frac{1}{1-C_1-C_2-C_3} - \frac{1}{C_3}}{1-C_1-C_2}}{C_2+C_3} \\ &\quad \left. + \frac{-\frac{\frac{1}{1+C_1+C_3} + \frac{1}{C_3}}{1+C_1} - \frac{\frac{1}{C_2+C_3} + \frac{1}{C_3}}{C_2} - \frac{\frac{1}{C_2+C_3} + \frac{1}{1+C_1+C_3}}{1+C_1+C_2}}{1+C_1+C_2+C_3} \right). \end{aligned} \quad (29)$$

The time scale t_d can now be estimated as described in Sec. III D. Evidently, also t_d depends on the parameters C_p , which we have to take into account when we minimize the cost function (26) for a given set of probabilities p_n , $n = 1, 2, 3$. For equal probabilities $p_n = 1/M$, we thus obtain $C_1 = 5.73$, $C_2 = 0.19$, and $C_3 = 6.07$. Optimizing these values iteratively we find $C_1 = 7.91$, $C_2 = 0.24$, and $C_3 = 8.78$. In Fig. 2 (c), we show the exact time evolution of the squared amplitudes of the lowest three instantaneous eigenstates. We note that in the lattice-gauge representation of this example, the degenerate ground states have Hamming distances $h_{13} = h_{23} = 3$ and $h_{12} = 4$. Thus, as discussed below Eq. (14), the instantaneous ground states $|\varphi_n(t)\rangle$ approach the states $|x_n\rangle$ for $t \rightarrow T$, and it is indeed the probabilities of these states at $t = T$ we want to control. The optimized C_p lead to final amplitudes $|a_1|^2 = 0.344$, $|a_2|^2 = 0.347$, and

$|a_3|^2 = 0.309$, close to their target values. We expect further improvement by including contributions of higher order in the effective Hamiltonian. For this model, the optimization of the C_p can be carried out exactly, i.e., using the iterative procedure described above with the *full* quantum dynamics. Then we obtain $C_1 = 9.31$, $C_2 = 0.40$, and $C_3 = 9.82$ with final probabilities almost exactly $1/M$ [Fig. 2 (c) solid line]. This demonstrates that the fidelity of the final state is not limited fundamentally but only by the accuracy with which we determine the control parameters. For the second example with probabilities shown in Fig. 2 (d), we obtain $C_1 = 5.53$, $C_2 = 0.86$, and $C_3 = 2.44$, and by iterative optimization $C_1 = 5.80$, $C_2 = 1.25$, and $C_3 = 2.68$, leading to $|a_1|^2 = 0.219$, $|a_2|^2 = 0.297$, and $|a_3|^2 = 0.484$. The exact results are again almost identical to the approximate solution. Let us stress two features of the

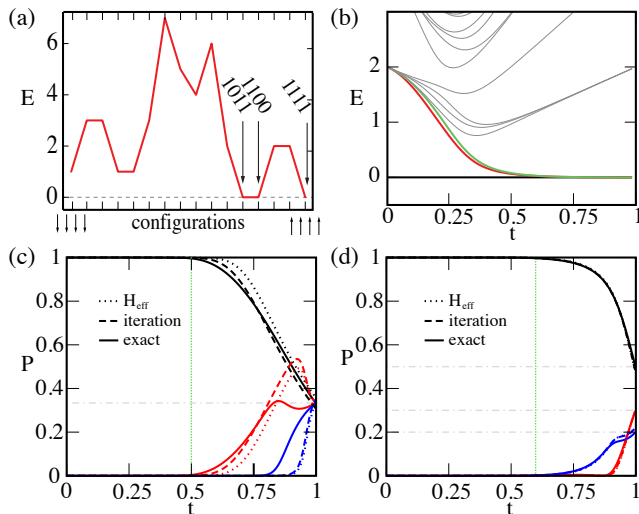


Figure 2. (a) Energy landscape of the classical spin model described in Sec. IV, which features global minima for configurations 1011, 1100 and 1111. The symmetry of global inversion can be broken by an additional local field. (b) The energy spectrum of the time-dependent Hamiltonian Eq. (1) shows a collapse to the degenerate states (black, red and green) of the final Hamiltonian. (c) Fair sampling: probabilities of the lowest M instantaneous eigenstates of the time-dependent Hamiltonian Eq. (1) for the example shown in Fig. 1. The time of diabaticity t_d from the effective model is $t_d \approx 0.5T$ (green dotted). The results from exact dynamics (solid), effective model (dotted) and improved iterative method (dashed) are all in good agreement. (d) Probabilities set to $p_1 = 0.2$, $p_2 = 0.3$, and $p_3 = 0.5$ with color code as in panel (c), where $t_d \approx 0.6T$. In (c) and (d), time is measured in units of T .

quantum dynamics: (i) The dynamics within the AMF is evidently adiabatic, i.e., the occupation of the instantaneous ground state is constant and close to unity, up to a time $t_d \approx 0.5$ and $t_d \approx 0.6$ in Figs. 2 (c) and 2 (d), respectively. (ii) This time t_d agrees well with the time at which the cost function, evaluated for the instantaneous ground state, takes its minimum — in line with the above claim that the desired state should be reached already at t_d and, in particular, prior to T .

B. Robustness to constraint errors

As we demonstrate systematically in the following, the final probabilities are rather robust to with respect to errors in the control parameters C_p . We define the relative error e , where $\hat{C}_p = eC_p$, and C_p are the constraints obtained by optimization as explained above. For the example given in Fig. 1 and target probabilities $p_n = 1/M$, the values for C_p are taken from the exact calculation with the full quantum dynamics. The changes in the probabilities for e ranging from 0.6 to 1.4 are shown in Fig. 3. Around $e = 1$, the solution is remarkably insensitive to errors.

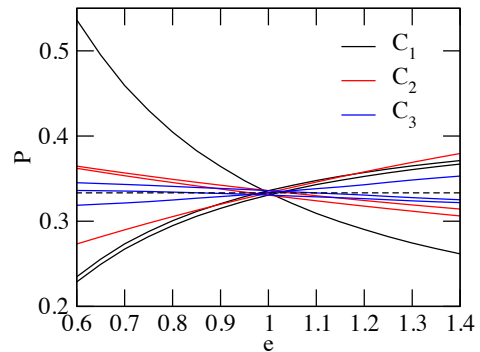


Figure 3. Probabilities P of the final superposition as a function of the relative error in the constraints e . We consider the example shown in Fig. 1 with equal target probabilities including errors in C_1 (black), C_2 (red) and C_3 (blue). The three lines of each color show the probabilities $|a_1|^2$, $|a_2|^2$, and $|a_3|^2$, respectively. For the constraint C_1 which is most sensitive to errors, the deviation in P is 10% for a error of 20% in C_1 . For other constraints the deviation in P is even smaller.

C. Ergodicity of the solution space

Finally, to address how general the method is, we ask whether it is possible to reach every combination of $|a_n|^2$ from the available parameters C_p and t_d . Let us count the number of degrees of freedom first: The number of constraints is $K - N + 1$ which grows quadratically with the length of the bit strings N , while the number of variables $|a_n|^2$ is $M - 1$ because of the normalization condition $\sum_{n=1}^M p_n = 1$. Thus, $M - 1$ degrees of freedom need to be programed and K degrees of freedom are available. This means that for large systems the number of available parameters will in general be large as compared to the number of variables that we want to program, leading us to expect that it should be possible to prepare any superposition.

For small systems, we can systematically address the question whether the solution hyperplane is ergodically populated from all constraint combinations. In the example introduced above, the number of bit strings is $M = 3$. With the condition $p_1 + p_2 + p_3 = 1$, the solution space is a two-dimensional plane in the three-dimensional space of probabilities. We can systematically check how this two-dimensional plane is populated from the following simplified model, illustrated in Fig. 4 (a). According to the effective model, we assume that the amplitudes in the instantaneous ground state stay constant after the freezing time t_d . We further assume that the freeze-in can be at any time during the protocol. Therefore, we can check each combination of C_1 , C_2 , and C_3 for each time t_d . We scanned the constraints in the interval 0.1 to 4.0 in steps of 0.1 and the time in steps of $T/30$. The resulting solution plane is shown in Fig. 4 (b). Even in this simplified model, the mapping is almost ergodic. For

larger systems we expect full ergodicity due to the larger number of degrees of freedom.

V. CONCLUSIONS

We presented a general framework that utilizes lattice-gauge degrees of freedom to control the dynamical preparation of a quantum superposition with tunable weights. The control parameters are determined from an effective multi-level Landau-Zener model. Our protocol can be implemented in state-of-the-art experiments, e.g., neutral atoms [20] or superconducting qubits [22]. From an application point of view, we hope this work is useful for quantum algorithms that benefit from data provided as superpositions [9]. The effective model also suggests a general answer to the question for the conditions of fair sampling [16, 18]. Our protocol opens several routes for extension, e.g., in combination with shortcut-to-adiabaticity methods [35–38], optimal control [39] and quantum approximate optimization algorithms [40]. An interesting challenge for future research is controlling not only the weights but also the phases in the final superposition state [41].

ACKNOWLEDGMENTS

We thank H. Katzgraber, S. Mandra, P. Zoller, P. Hauke, H. Neven, N. Ding, M. Mohseni, S. Gazit, M. Serbyn, and E. Altman for fruitful discussions. Research was funded by the Austrian Science Fund (FWF) through a START grant under Project No. Y1067-N27, the Hauser-Raspe foundation, and by the ERC through the synergy grant UQUAM.

Appendix A: Effective Hamiltonian for the example in Sec. IV

Using Eq. (22), it is straightforward to calculate $H_{\text{eff}}(t)$ numerically. However, for the simple example considered in Sec. IV, we find it instructive to obtain explicit expressions for the matrix elements of $H_{\text{eff}}(t)$ by hand. This also clarifies how the constraint strengths C_p enter $H_{\text{eff}}(t)$ and thus allow us to control the quantum dynamics.

For the model introduced in Fig. 1 of the main text, the part of the Hamiltonian involving the constraints involves two three-body and one four-body interaction,

$$H_C = -C_1 \sigma_1^z \sigma_2^z \sigma_4^z - C_2 \sigma_2^z \sigma_3^z \sigma_5^z - C_3 \sigma_2^z \sigma_4^z \sigma_5^z \sigma_6^z. \quad (\text{A1})$$

Equivalently, the three-body terms can be viewed as four-body terms in which one spin is held fixed, e.g., by an external field [19]. We denote by S_i the set of constraints that involve spin i ,

$$\begin{aligned} S_1 &= \{1\}, & S_2 &= \{1, 2, 3\}, & S_3 &= \{2\}, \\ S_4 &= \{1, 3\}, & S_5 &= \{2, 3\}, & S_6 &= \{3\}. \end{aligned} \quad (\text{A2})$$

The energy of the degenerate ground states $|z_n\rangle$ is

$$E_0 = -\frac{t}{T} \left(\sum_i J_i z_{n,i} + \sum_{p=1}^3 C_p \right), \quad (\text{A3})$$

where the contribution due to the local fields depends on the orientation of the spins $z_{n,i}$ (here, we replace $z_{n,i} = 0, 1 \rightarrow \pm 1$), while each constraint contributes with $-tC_p/T$ to lowering the energy of states in the ground-state manifold.

We obtain the diagonal elements of H_{eff} at second-order in perturbation theory:

$$\begin{aligned} H_{\text{eff},nn} &= E_0 + \left(1 - \frac{t}{T}\right)^2 \sum_{i,j} \langle z_n | \sigma_i^x \frac{1}{E_0 - H_0} \sigma_j^x | z_n \rangle \\ &= E_0 + \left(1 - \frac{t}{T}\right)^2 \sum_i \frac{1}{E_0 - \langle z_n | \sigma_i^x H_0 \sigma_i^x | z_n \rangle}. \end{aligned} \quad (\text{A4})$$

Here we used that the state $\sigma_i^x |z_n\rangle$ is still a product state in the σ^z -basis (only with spin i flipped relative to $|z_n\rangle$), and H_0 is diagonal in this basis. The excitation energy of the state $\sigma_i^x |z_n\rangle$ is given by

$$\langle z_n | \sigma_i^x H_0 \sigma_i^x | z_n \rangle - E_0 = \frac{2t}{T} \left(J_i z_{n,i} + \sum_{p \in S_i} C_p \right), \quad (\text{A5})$$

i.e., we get a contribution from the local field acting on spin i and from all the constraints that involve this same spin. These constraints are satisfied in the state $|z_n\rangle$ and therefore violated if the single spin i is flipped. Hence,

$$H_{\text{eff},nn} = E_0 - \frac{T}{2t} \left(1 - \frac{t}{T}\right)^2 \sum_i \frac{1}{J_i z_{n,i} + \sum_{p \in S_i} C_p}. \quad (\text{A6})$$

For the off-diagonal elements $H_{\text{eff},nn'}$ there is no equally compact form. However, they can be visualized in an intuitive way. The key observation is that a given order of the perturbation, applied to a state $|z_{n'}\rangle$ leads to “paths” originating from this state. The length of these paths is the number of single spin flips to go from one state to the other, and the required order of perturbation theory is determined by the length of paths connecting two states $|z_{n'}\rangle$ and $|z_n\rangle$: To leading order, those paths contribute to $H_{\text{eff},nn'}$ that connect the states $|z_{n'}\rangle$ and $|z_n\rangle$ in the minimum number of steps. This number is given by the Hamming distance $h_{nn'}$ of these states.

In our example, two of the degenerate ground states of H_0 are given by $|z_n\rangle = |010011\rangle$ and $|z_{n'}\rangle = |001001\rangle$, i.e., they have Hamming distance $h_{nn'} = 3$. In particular, $|z_n\rangle$ can be obtained from $|z_{n'}\rangle$ by flipping the spins at positions 2, 3, and 5, $|z_n\rangle = \sigma_2^x \sigma_3^x \sigma_5^x |z_{n'}\rangle$. Then, there is an off-diagonal matrix element $H_{\text{eff},nn'}$ in third order in perturbation theory. As explained above, the terms contributing to this matrix element can be visualized as sums over paths connecting the states $|z_n\rangle$ and

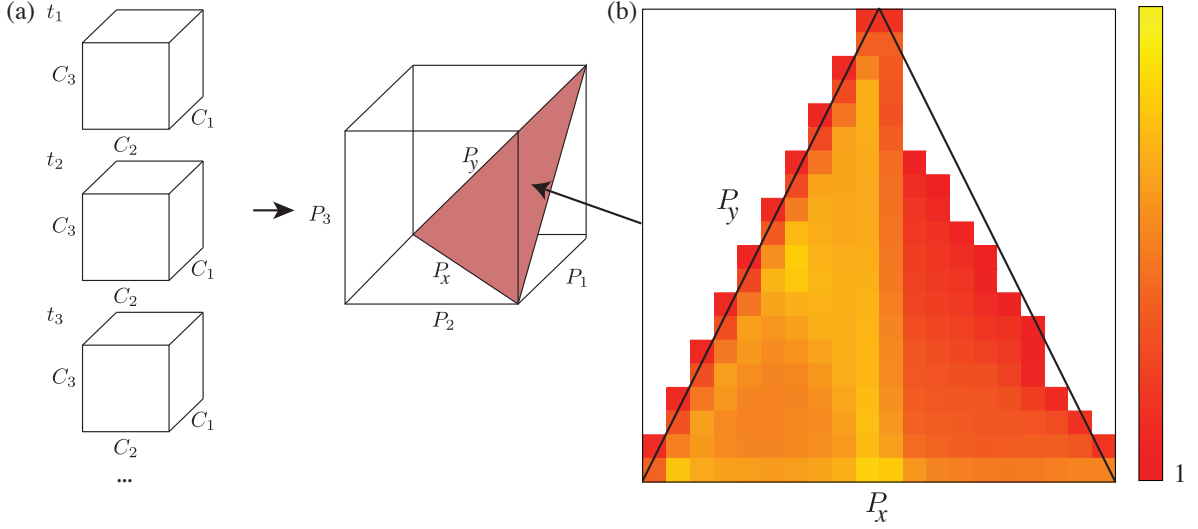
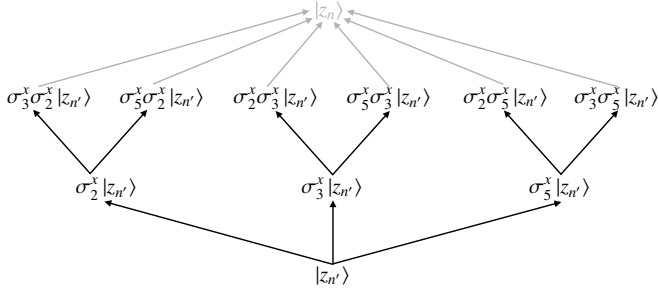


Figure 4. (a) Our protocol maps the parameter set $\{t_d, C_1, C_2, C_3\}$ to a two-dimensional plane in the solution space spanned by $\{p_1, p_2, p_3\}$. The mapping is ergodic, if each point on this plane can be reached. (b) Heatmap of the projected probabilities on the two-dimensional solution plane. Points that can be reached (red) are all within the expected triangle, while a small region in the top right (white) cannot be reached.

$|z_{n'}\rangle$. Each path corresponds to a particular order in which the spins 2, 3, and 5 are flipped, and each segment of a given path contributes with a factor of minus one over the excitation energy of the state at the end of the segment,



The tree-like structure of the diagram translates directly to the iterated fractions, e.g., in the expression for g_{13} in Eq. (28). Indeed, comparing the first term in g_{13} and the left-most branch of the tree, we see that flipping spin 2 leads to a state with excitation energy $2(1 + C_1 + C_2 + C_3)$; depending on which spin is flipped next, states with energies of $2(1 + C_1)$ or $2(C_2 + C_3)$ are reached. The last segment of the path that leads to $|z_n\rangle$ does not contribute to the matrix element $H_{\text{eff},nn'}$ as is indicated in the diagram by reduced opacity.

We formalize these considerations in the following. Let's denote the spins we have to flip to get from $|z_{n'}\rangle$ to

$|z_n\rangle$ by $D = (i_1, i_2, \dots, i_h)$ with $h = h_{nn'}$. The paths that contribute to $H_{\text{eff},nn'}$ are different sequences of spin flips, i.e., permutations of D . We denote such a permutation by $\pi(D) = (i_{\pi_1}, \dots, i_{\pi_h})$. There are $h!$ permutations. For a given permutation, the repeated action of the perturbation V takes us through the sequence of states

$$|z_{n'}\rangle \rightarrow \sigma_{i_{\pi_1}}^x |z_{n'}\rangle \rightarrow \sigma_{i_{\pi_2}}^x \sigma_{i_{\pi_1}}^x |z_{n'}\rangle \rightarrow \dots \rightarrow \sigma_{i_{\pi_h}}^x \dots \sigma_{i_{\pi_1}}^x |z_{n'}\rangle = |z_n\rangle. \quad (\text{A7})$$

Using the same notation as in Eq. (A4), we find

$$H_{\text{eff},nn'} = (-1)^h \left(1 - \frac{t}{T}\right)^h \times \sum_{\pi} \frac{1}{E_0 - \langle z_{n'} | \sigma_{i_{\pi_1}}^x \dots \sigma_{i_{\pi_{h-1}}}^x H_0 \sigma_{i_{\pi_{h-1}}}^x \dots \sigma_{i_{\pi_1}}^x | z_{n'} \rangle} \times \dots \frac{1}{E_0 - \langle z_{n'} | \sigma_{i_{\pi_1}}^x H_0 \sigma_{i_{\pi_1}}^x | z_{n'} \rangle}. \quad (\text{A8})$$

The constraint strengths C_p enter this expression through the energy denominators as above in Eq. (A6). While Eqs. (A6) and (A8) provide valuable insight into the general structure of the effective model, for doing any practical calculation it is much simpler to directly implement Eq. (22), e.g., in MATHEMATICA. Doing this for our model, we find the explicit expressions for the coefficients e_n and $g_{nn'}$ reported in Eqs. (27), (28), and (29).

[1] J Ignacio Cirac and Peter Zoller, "Goals and opportunities in quantum simulation," *Nat. Phys.* **8**, 264–266

(2012).

- [2] Immanuel Bloch, Jean Dalibard, and Sylvain Nascimbene, “Quantum simulations with ultracold quantum gases,” *Nat. Phys.* **8**, 267–276 (2012).
- [3] I. M. Georgescu, S. Ashhab, and Franco Nori, “Quantum simulation,” *Rev. Mod. Phys.* **86**, 153–185 (2014).
- [4] Chr. Wunderlich, Th. Hannemann, T. Körber, H. Häffner, C. F. Roos, W. Hänsel, R. Blatt, and F. Schmidt-Kaler, “Robust state preparation of a single trapped ion by adiabatic passage,” *J. Mod. Opt.* **54**, 1541–1549 (2007).
- [5] Johannes Zeiher, Rick van Bijnen, Peter Schausz, Sebastian Hild, Jae-yoon Choi, Thomas Pohl, Immanuel Bloch, and Christian Gross, “Many-body interferometry of a Rydberg-dressed spin lattice,” *Nat. Phys.* **12**, 1095–1099 (2016).
- [6] L. DiCarlo, M. D. Reed, L. Sun, B. R. Johnson, J. M. Chow, J. M. Gambetta, L. Frunzio, S. M. Girvin, M. H. Devoret, and R. J. Schoelkopf, “Preparation and measurement of three-qubit entanglement in a superconducting circuit,” *Nature* **467**, 574–578 (2010).
- [7] H. Bernien, S. Schwartz, A. Keesling, H. Levine, A. Omran, H. Pichler, S. Choi, A. S. Zibrov, M. Endres, M. Greiner, V. Vuletić, and M. D. Lukin, “Probing many-body dynamics on a 51-atom quantum simulator,” ArXiv e-prints (2017), [arXiv:1707.04344](https://arxiv.org/abs/1707.04344) [quant-ph].
- [8] J. M. Raimond, M. Brune, and S. Haroche, “Manipulating quantum entanglement with atoms and photons in a cavity,” *Rev. Mod. Phys.* **73**, 565–582 (2001).
- [9] Vittorio Giovannetti, Seth Lloyd, and Lorenzo Maccone, “Quantum random access memory,” *Phys. Rev. Lett.* **100**, 160501 (2008).
- [10] Vittorio Giovannetti, Seth Lloyd, and Lorenzo Maccone, “Architectures for a quantum random access memory,” *Phys. Rev. A* **78**, 052310 (2008).
- [11] S. Lloyd, M. Mohseni, and P. Rebentrost, “Quantum algorithms for supervised and unsupervised machine learning,” ArXiv e-prints (2013), [arXiv:1307.0411](https://arxiv.org/abs/1307.0411) [quant-ph].
- [12] Tadashi Kadowaki and Hidetoshi Nishimori, “Quantum annealing in the transverse ising model,” *Phys. Rev. E* **58**, 5355–5363 (1998).
- [13] E. Farhi, J. Goldstone, S. Gutmann, and M. Sipser, “Quantum Computation by Adiabatic Evolution,” ArXiv e-prints (2000), [arXiv:quant-ph/0001106](https://arxiv.org/abs/quant-ph/0001106) [quant-ph].
- [14] Mohammad H. Amin, “Searching for quantum speedup in quasistatic quantum annealers,” *Phys. Rev. A* **92**, 052323 (2015).
- [15] Sergio Boixo, Vadim N Smelyanskiy, Alireza Shabani, Sergei V Isakov, Mark Dykman, Vasil S Denchev, Mohammad H Amin, Anatoly Yu Smirnov, Masoud Mohseni, and Hartmut Neven, “Computational multi-qubit tunnelling in programmable quantum annealers,” *Nat. Commun.* **7**, 1–7 (2016), [arXiv:arXiv:1411.4036v2](https://arxiv.org/abs/1411.4036v2).
- [16] Yoshiki Matsuda, Hidetoshi Nishimori, and Helmut G Katzgraber, “Ground-state statistics from annealing algorithms: quantum versus classical approaches,” *New J. Phys.* **11**, 073021 (2009).
- [17] Sergio Boixo, Troels F. Ronnow, Sergei V. Isakov, Zhihui Wang, David Wecker, Daniel A. Lidar, John M. Martinis, and Matthias Troyer, “Evidence for quantum annealing with more than one hundred qubits,” *Nat Phys* **10**, 218–224 (2014).
- [18] Salvatore Mandrà, Zheng Zhu, and Helmut G. Katzgraber, “Exponentially biased ground-state sampling of quantum annealing machines with transverse-field driving hamiltonians,” *Phys. Rev. Lett.* **118**, 070502 (2017).
- [19] Wolfgang Lechner, Philipp Hauke, and Peter Zoller, “A quantum annealing architecture with all-to-all connectivity from local interactions,” *Science Advances* **1** (2015).
- [20] Alexander W Glaetzle, Rick MW van Bijnen, Peter Zoller, and Wolfgang Lechner, “A coherent quantum annealer with rydberg atoms,” *Nature Communications* **8** (2017).
- [21] A. Rocchetto, S. C. Benjamin, and Y. Li, “Stabilisers as a design tool for new forms of Lechner-Hauke-Zoller Annealer,” ArXiv e-prints (2016), [arXiv:1603.08554](https://arxiv.org/abs/1603.08554) [quant-ph].
- [22] Shruti Puri, Samuel Boutin, and Alexandre Blais, “Engineering the quantum states of light in a kerr-nonlinear resonator by two-photon driving,” *npj Quantum Information* **3**, 18 (2017).
- [23] Martin Leib, Peter Zoller, and Wolfgang Lechner, “A transmon quantum annealer: Decomposing many-body ising constraints into pair interactions,” *Quantum Science and Technology* **1**, 015008 (2016).
- [24] Itay Hen, Joshua Job, Tameem Albash, Troels F. Ronnow, Matthias Troyer, and Daniel A. Lidar, “Probing for quantum speedup in spin-glass problems with planted solutions,” *Phys. Rev. A* **92**, 042325 (2015).
- [25] John J Hopfield, “Neural networks and physical systems with emergent collective computational abilities,” *Proceedings of the national academy of sciences* **79**, 2554–2558 (1982).
- [26] To be published.
- [27] T.W.B. Kibble, “Some implications of a cosmological phase transition,” *Phys. Rep.* **67**, 183–199 (1980); “Topology of cosmic domains and strings,” *J. Phys. A. Math. Gen.* **9**, 1387–1398 (2001); W.H. Zurek, “Cosmological experiments in superfluid helium?” *Nature* **317**, 505–508 (1985); “Cosmic Strings in Laboratory Superfluids and the Topological Remnants of Other Phase Transitions,” *Acta Phys. Pol. B* **24**, 1301 (1993); “Cosmological experiments in condensed matter systems,” *Phys. Rep.* **276**, 177–221 (1996).
- [28] Bogdan Damski, “The simplest quantum model supporting the kibble-zurek mechanism of topological defect production: Landau-zener transitions from a new perspective,” *Phys. Rev. Lett.* **95**, 035701 (2005), [arXiv:0411004](https://arxiv.org/abs/0411004) [cond-mat].
- [29] J R Schrieffer and P A Wolff, “Relation between the Anderson and Kondo Hamiltonians,” *Phys. Rev.* **149**, 491–492 (1966).
- [30] As described in Sec. III C, both $H_{\text{eff}}(t)$ and $U_{\text{SW}}(t)$ can be expressed as perturbative expansions in $1-t/T$; then, for each term of order $(1-t/T)^n$ in $H_{\text{eff}}(t)$, the corresponding term in $U_{\text{SW}}(t)U_{\text{SW}}^\dagger(t)$ is of order $(1/T)(1-t/T)^{n-1}$. To determine the control parameters for the protocol, we evaluate the effective Hamiltonian at t_a , which is typically a finite fraction of T . Then, $1/T \ll 1-t_a/T$, and the second term in $B_{nn'}(t)$ can safely be neglected.
- [31] C De Grandi and A Polkovnikov, “Quantum Quenching, Annealing and Computation,” (Springer Berlin Heidelberg, Berlin, Heidelberg, 2010) Chap. Adiabatic Perturbation Theory: From Landau-Zener Problem to Quenching Through a Quantum Critical Point, pp. 75–114.
- [32] Sergey Bravyi, David P. DiVincenzo, and Daniel Loss, “SchriefferWolff transformation for quantum many-body systems,” *Ann. Phys. (N. Y.)* **326**, 2793–2826 (2011).

- [33] Landau L D and Lifshitz E M, *Quantum Mechanics: Non-relativistic Theory*, 3rd ed. (Pergamon Press, Oxford, 1977).
- [34] Note, that the minimum $\Omega(\{a_n\}) = 0$ can only be reached if there are no transitions out of the AMF.
- [35] M V Berry, “Transitionless quantum driving,” *J. Phys. A Math. Theor.* **42**, 365303–9 (2009).
- [36] Sebastian Deffner, Christopher Jarzynski, and Adolfo del Campo, “Classical and Quantum Shortcuts to Adiabaticity for Scale-Invariant Driving,” *Phys. Rev. X* **4**, 021013 (2014).
- [37] Dries Sels and Anatoli Polkovnikov, “Minimizing irreversible losses in quantum systems by local counterdiabatic driving.” *Proc. Natl. Acad. Sci. U. S. A.* **114**, E3909–E3916 (2017).
- [38] Ayoti Patra and Christopher Jarzynski, “Shortcuts to adiabaticity using flow fields,” (2017), [arXiv:1707.01490](https://arxiv.org/abs/1707.01490).
- [39] T. Caneva, M. Murphy, T. Calarco, R. Fazio, S. Montangero, V. Giovannetti, and G. E. Santoro, “Optimal control at the quantum speed limit,” *Phys. Rev. Lett.* **103**, 240501 (2009).
- [40] Edward Farhi, Jeffrey Goldstone, and Sam Gutmann, “A Quantum Approximate Optimization Algorithm,” *arXiv Prepr. arXiv1411.4028*, 1–16 (2014), [arXiv:1411.4028](https://arxiv.org/abs/1411.4028).
- [41] S. P. Jordan, K. S. M. Lee, and J. Preskill, “Quantum Algorithms for Quantum Field Theories,” *Science* (80-). **336**, 1130–1133 (2012), [arXiv:arXiv:1111.3633v2](https://arxiv.org/abs/1111.3633v2).